IEEE Access
Multidisciplinary | Rapid Review | Open Access Journal

Received May 31, 2018, accepted July 9, 2018, date of publication July 13, 2018, date of current version August 7, 2018.

Digital Object Identifier 10.1109/ACCESS.2018.2855965

Underwater Electro-Location Method Based on Improved Matrix Adaptation Evolution Strategy

YIDONG XU[1], LILI GUO[1], (Member, IEEE), WENJING SHANG[1], AND YINGSONG LI[1,2], (Member, IEEE)

[1]College of Information and Communication Engineering, Harbin Engineering University, Harbin 150001, China
[2]National Space Science Center, Chinese Academy of Sciences, Beijing 100190, China

Corresponding author: Yingsong Li (liyingsong@ieee.org)

This work was supported in part by the National Key Research and Development Program of China-Government Corporation Special Program under Grant 2016YFE0111100, in part by the Science Foundation of Heilongjiang Province under Grant QC2015075, in part by the Fundamental Research Funds for the Central Universities under Grant HEUCFG201829, and in part by the Opening Fund of Acoustics Science and Technology Laboratory under Grant SSKF2016001.

ABSTRACT In this paper, a new locating method based on the optimization method for estimating the position of an electric dipole source in underwater environments with a plate uniform circular antenna (PUCA) is presented. The image principle is introduced to build the manifold of the PUCA, greatly reducing the complexity of the manifold. The evaluation function is obtained using the mixed polarization multiple signal classification algorithm, where the minimum value is found using the fast optimal method improved matrix adaptation evolution strategy (MA-ES). In this locating method, the voltage from each channel of the PUCA is the input spatial-temporal data. As a result, the 3-D field components are reduced, and the method can easily be implemented in practical engineering applications. The theoretical analysis and the experiments conducted for both the simulation and the actual received data demonstrate that the accuracy performance of the locating method based on the improved MA-ES is higher than that of the MA-ES and of the covariance MA-ES.

INDEX TERMS Electro-location, underwater, improved MA-ES, PUCA.

I. INTRODUCTION

In the context of underwater exploration, such as deep sea exploration and rescue missions in catastrophic conditions, it is important to estimate the target position. Currently, underwater target location continues to be challenging in theory and in engineering practice [1]–[3]. In both cases, a new locating method is required that is easy to compute and designed for a broad class of underwater locating systems. In recent years, various underwater locating technologies have been proposed, including acoustic-, light- and map-based locating methods [4]–[6]. At present, sonar locating methods dominate the field in underwater target locating applications [4], [7], [8]. However, the locating performance of the sonar method degrades in specific cases, such as in environments with heterogeneous distributions of temperature or density, when the background noise is high, in complex geomorphic structures and in the presence of the Doppler effect [5], [9]. The locating accuracy of underwater imaging based on light depends on the transparency of water and, therefore, cannot work in turbid water or in environments with no light [6]. To overcome these drawbacks, underwater target locating methods based on electromagnetic fields have received research attention. Because the electromagnetic field has much higher velocity than the sound wave, the electromagnetic field-based localization method does not suffer from the Doppler effect nor does it require transparent water [10], [11]. Generally, the electromagnetic noise is extremely low and stable. This is especially true in deep ocean environments because of the high conductivity of seawater [12], [13].

There are two primary electromagnetic field-based underwater locating method systems, i.e., the electromagnetic wave locating method and the low-frequency electro-locating method. In the literature [10], [14], locating methods are proposed based on the power path loss model of an electromagnetic wave propagating through seawater. However, the skin depth of the high frequency signal is small in seawater. Therefore, the radio-frequency signal power decreases dramatically, reducing its applicability in wide range locating. Locating methods based on quasi-static electric fields have

been investigated [1], [2], [15], [16], resulting in lower path losses compared with the high-frequency signals in seawater. These electric sense active locating methods are inspired by weak electric fish, which are able to find and locate a target by sensing the electric field distortion in dark and turbid environments. The electric sense locating methods show good performance in underwater avoidance, docking and close-range object shape estimation. However, the electric field re-emitted by objects is usually much weaker than that of the source field. Therefore, electric sense active locating methods are not suitable for long distance target locating scenarios. The MUltiple SIgnal Classification (MUSIC) algorithm is a noniterative algorithm that creates a space spectrum to locate an underwater electromagnetic source. MUSIC-type algorithms can be introduced when we are only interested in the position of the target, which can reduce the computation time [17], [18]. To estimate the position of a small target in two-dimensional space, a MUSIC-type algorithm has been proposed by Ammari *et al.* [19]. In their study, the far field scattering signal is sampled as the locating data. However, the far-field signal is a radio-frequency signal, which suffers from significant power losses in seawater.

In our previous works [18], [20], passive and active locating methods based on the boundary element method (BEM) forward model have been proposed. The BEM-based forward model requires a large amount of computational resources because of the operations by the high-order impedance matrix. Moreover, the uniform mesh grid scan method are applied when searching the global maximum in three-dimensional space, which also results in large calculation burden. To simplify the forward model and reduce the computation burden, in this paper, we propose a novel solution for underwater locating based on the image principle and the improved matrix adaptation evolution strategy (MA-ES). In this method, we first design a PUCA, which acts as the electric signal receiving array. In this PUCA, $(M+1)$ electrodes are situated on an insulator plate. The $(M+1)$th electrode is set as the electric potential reference point, which is situated at the center of the insulator plate. The remainder of the electrodes are evenly arranged on the circumference of the insulator plate, surrounding the reference point. With this design, the voltage between the reference point and the other electrodes is measured directly. The image principle is introduced to yield the forward potential distribution model of the PUCA, which features lower complexity and a lower computation burden compared with the BEM and finite element method (FEM). MP-MUSIC is applied while locating the target, which can handle signals with polarization. The three-dimensional target position can be estimated by minimizing the generalized eigenvalue (the gain matrix and the project matrix of the noise subspace) [21]. Finding the minimum eigenvalue is an optimization problem, indicating that use of a suitable optimization method can significantly reduce the calculation time. The improved MA-ES is introduced to find the minimum eigenvalue, which combines the characteristics of evolution strategies and the Gaussian modeling of the best solutions [22], [23]. A set of physical experiments in the laboratory is performed to verify the proposed locating method. The experimental results indicate that the proposed locating method yields high accuracy estimations in underwater target locating.

II. UNDERWATER TARGET ELECTRO-LOCATING METHOD

We suppose that a source target is emitting a monochromatic signal at frequency f from a position $\boldsymbol{r}_{\mathrm{t}} \in \mathbb{R}^{N\times 1}$, where N is the position dimension. In underwater locating applications, $N = 3$. The potential signal is measured by the passive PUCA, composed of $(M+1)$ electrodes. Let $\boldsymbol{\Psi} \in \mathbb{R}^{(M+1)\times 1}$ be the measured voltage of each channel. Our goal is to assess the measured voltage $\boldsymbol{\Psi}$ at position $\boldsymbol{r}_{\mathrm{t}}$. In practical applications, several snapshots are needed for underwater target localization. For clarity, a high signal-to-noise ratio (SNR) signal output strategy based on a narrow band filter is performed, yielding the locating method for a single snapshot [4].

Locating a target in an underwater environment is an inversion problem, which can be considered an optimization problem as follows:

$$\boldsymbol{r}_{\mathrm{t}} = \arg \min_{\boldsymbol{r}_{\mathrm{t}}} J(\boldsymbol{\Psi}, f(\boldsymbol{r}_{\mathrm{t}})) \tag{1}$$

where J is the evaluation function, which measures how much the estimated result given by the forward model $f(\boldsymbol{r}_{\mathrm{t}})$ fits the measured voltage $\boldsymbol{\Psi}$. Hence, in order to locate the source target underwater, three major problems must be solved: 1) a suitable forward model $f(\boldsymbol{r}_{\mathrm{t}})$ is needed, which can provide accurate estimations of the voltage for each channel of the PUCA; an analytical expression for $f(\boldsymbol{r}_{\mathrm{t}})$ is derived based on the electromagnetic field propagation model; 2) an appropriate evaluation function J should be chosen; in radar technology and underwater acoustic locating applications, a signal subspace projection using eigen-decomposition is widely used [24], [25]; and 3) the search time for the global optimal solution should be reduced while avoiding local optimum solutions. In most cases, the grid search method, a genetic algorithm (GA), a gradient algorithm, etc., is used to minimize the evaluation function J. However, the grid search method spends a large amount of computation time searching, especially for a high-dimensional optimization problem, and the gradient algorithm suffers from the appearance of local solutions for non-convex optimization problems. Moreover, GA requires long time calculations for convergence.

A. UNDERWATER ELECTRIC FIELD FORWARD MODEL

To locate the target underwater, the electric field distribution or the forward model $f(\boldsymbol{r}_{\mathrm{t}})$ must first be analyzed. We consider an infinite half-space with Neumann boundary conditions, as indicated in Figure 1. The insulator can be a dielectric material, such as plastic or glass. The conducting material is seawater, with conductivity σ. If the electric dipole source is located at position $\boldsymbol{r}_{\mathrm{t}}$, with the dipole moment of $\boldsymbol{p}$, then the basic image principle from electrostatic field theory

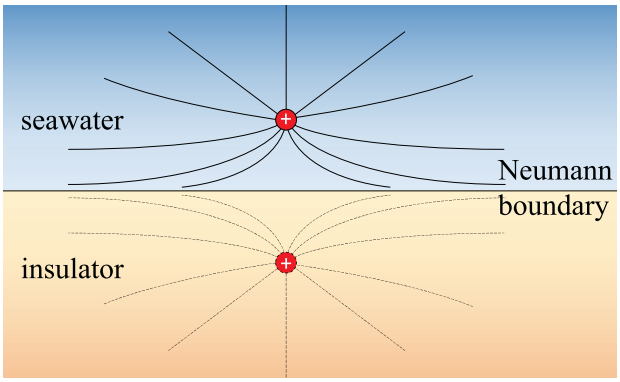

FIGURE 1. The field distribution for an electric source in seawater with Neumann boundary conditions.

is applied to yield the potential $\phi_{\boldsymbol{r}}$ at point $\boldsymbol{r}$ on the boundary as follows:

$$\phi_{\boldsymbol{r}} = \frac{\boldsymbol{p} \cdot (\boldsymbol{r} - \boldsymbol{r}_{\mathrm{t}})}{2\pi\sigma\,|\boldsymbol{r} - \boldsymbol{r}_{\mathrm{t}}|^3} \tag{2}$$

The $M+1$ electrodes are situated at positions $\boldsymbol{r}_i$, where $i = 1, 2, 3, \cdots, M+1$. We define the $(M+1)$th electrode as the reference point $\boldsymbol{r}_{\mathrm{ref}}$. The voltage between the reference point and the other electrodes $\boldsymbol{\Psi}$ can be expressed as:

$$\boldsymbol{\Psi} = \boldsymbol{\Phi}_r - \boldsymbol{\Phi}_{\mathrm{ref}} = (\mathbf{G}_r - \mathbf{G}_{\mathrm{ref}})\boldsymbol{p}; \tag{3}$$

$$\begin{aligned}\boldsymbol{\Phi}_r &= \mathbf{G}_r\boldsymbol{p} \\ &= \frac{1}{2\pi\sigma}\begin{bmatrix} \frac{\boldsymbol{e}_x\cdot(\boldsymbol{r}_1-\boldsymbol{r}_{\mathrm{t}})}{|\boldsymbol{r}_1-\boldsymbol{r}_{\mathrm{t}}|^3} & \frac{\boldsymbol{e}_y\cdot(\boldsymbol{r}_1-\boldsymbol{r}_{\mathrm{t}})}{|\boldsymbol{r}_1-\boldsymbol{r}_{\mathrm{t}}|^3} & \frac{\boldsymbol{e}_z\cdot(\boldsymbol{r}_1-\boldsymbol{r}_{\mathrm{t}})}{|\boldsymbol{r}_1-\boldsymbol{r}_{\mathrm{t}}|^3} \\ \frac{\boldsymbol{e}_x\cdot(\boldsymbol{r}_2-\boldsymbol{r}_{\mathrm{t}})}{|\boldsymbol{r}_2-\boldsymbol{r}_{\mathrm{t}}|^3} & \frac{\boldsymbol{e}_y\cdot(\boldsymbol{r}_2-\boldsymbol{r}_{\mathrm{t}})}{|\boldsymbol{r}_2-\boldsymbol{r}_{\mathrm{t}}|^3} & \frac{\boldsymbol{e}_z\cdot(\boldsymbol{r}_2-\boldsymbol{r}_{\mathrm{t}})}{|\boldsymbol{r}_2-\boldsymbol{r}_{\mathrm{t}}|^3} \\ & \ddots & \\ \frac{\boldsymbol{e}_x\cdot(\boldsymbol{r}_M-\boldsymbol{r}_{\mathrm{t}})}{|\boldsymbol{r}_M-\boldsymbol{r}_{\mathrm{t}}|^3} & \frac{\boldsymbol{e}_y\cdot(\boldsymbol{r}_M-\boldsymbol{r}_{\mathrm{t}})}{|\boldsymbol{r}_M-\boldsymbol{r}_{\mathrm{t}}|^3} & \frac{\boldsymbol{e}_z\cdot(\boldsymbol{r}_M-\boldsymbol{r}_{\mathrm{t}})}{|\boldsymbol{r}_M-\boldsymbol{r}_{\mathrm{t}}|^3} \end{bmatrix} \\ &\quad\times\begin{bmatrix} p_x \\ p_y \\ p_z \end{bmatrix}\end{aligned} \tag{4}$$

$$\begin{aligned}\boldsymbol{\Phi}_{\mathrm{ref}} &= \mathbf{G}_{\mathrm{ref}}\boldsymbol{p} \\ &= \frac{1}{2\pi\sigma}\begin{bmatrix}1\\1\\\vdots\\1\end{bmatrix}_{M\times 1}\begin{bmatrix} \frac{\boldsymbol{e}_x\cdot(\boldsymbol{r}_{\mathrm{ref}}-\boldsymbol{r}_{\mathrm{t}})}{|\boldsymbol{r}_{\mathrm{ref}}-\boldsymbol{r}_{\mathrm{t}}|^3} \\ \frac{\boldsymbol{e}_y\cdot(\boldsymbol{r}_{\mathrm{ref}}-\boldsymbol{r}_{\mathrm{t}})}{|\boldsymbol{r}_{\mathrm{ref}}-\boldsymbol{r}_{\mathrm{t}}|^3} \\ \frac{\boldsymbol{e}_z\cdot(\boldsymbol{r}_{\mathrm{ref}}-\boldsymbol{r}_{\mathrm{t}})}{|\boldsymbol{r}_{\mathrm{ref}}-\boldsymbol{r}_{\mathrm{t}}|^3} \end{bmatrix}^{\mathrm{T}}\begin{bmatrix} p_x \\ p_y \\ p_z \end{bmatrix}\end{aligned} \tag{5}$$

where $\boldsymbol{e}_x$,$\boldsymbol{e}_y$ and $\boldsymbol{e}_z$ are the normal vectors in the x, y and z directions. In addition, $\boldsymbol{p} = \begin{bmatrix} p_x & p_y & p_z \end{bmatrix}^{\mathrm{T}}$. In the expressions above, the $(M \times 3)$ matrix $\mathbf{G} = \mathbf{G}_r - \mathbf{G}_{\mathrm{ref}}$ is referred to as the gain matrix or array manifold [26]. Equation (3) shows that $\mathbf{G}$ is the array manifold with the following arguments: the electric dipole source position $\boldsymbol{r}_{\mathrm{t}}$, the electrode position $\boldsymbol{r}$ and the conductivity of the seawater σ. We rewrite the gain matrix as $\widetilde{\mathbf{G}} = \sigma\mathbf{G}$ and the source dipole moment as $\widetilde{\boldsymbol{p}} = \frac{\boldsymbol{p}}{\sigma}$. As a result, $\widetilde{\mathbf{G}}$ is the new gain matrix without the parameter σ. In this section, the forward model f is derived for an electric dipole source in an infinite half space, with which the voltage between two electrodes located at the boundary can be readily obtained.

B. THE EVALUATION FUNCTION BASED ON MP-MUSIC

The electric field excited by an electric dipole source in seawater is polarized because the different azimuth of the dipole moment yields totally different field and voltage at the receiving electrodes. To estimate the position of the electric dipole source in the seawater, the MP-MUSIC algorithm is introduced as the evaluation function J, which is a high-accuracy locating algorithm based on a subspace algorithm [27], [28]. It is not necessary to calculate the azimuth of the polarized incident signals, which can also be applied for underwater target locating. The canonical MUSIC algorithm is widely used in direction-of-arrival (DOA) area estimation. The phase of the incident wave is the primary argument to consider. In this study, the locating method is different from the canonical MUSIC algorithm. Because we estimate the three-dimensional position of the target according to the received quasi-static electric signal from the PUCA, the voltage amplitude, not the phase, contains the target position information. Suppose that the relative displacement of the PUCA system and the electric dipole source can be neglected during the measurements. For each snapshot, the measured data are acquired as $\boldsymbol{\Psi} = \mathbf{G}\boldsymbol{p} + \boldsymbol{e}$, where the additive noise matrix $\boldsymbol{e}$ is assumed to have a zero mean with covariance $E\left\{\boldsymbol{e}\boldsymbol{e}^{\mathrm{H}}\right\} = {\sigma_e}^2\mathbf{I}$, where $E\{\cdot\}$ is the expected value of the argument, $(\cdot)^{\mathrm{H}}$ denotes the Hermitian transpose operator, and $\mathbf{I}$ denotes the identity matrix.

According to the MP-MUSIC algorithm, the array covariance matrix $\boldsymbol{\Psi}$ under the zero-mean white noise assumption based on the one snapshot acquired voltage $\boldsymbol{\Psi}$ is as follows:

$$\mathbf{R}_{\boldsymbol{\Psi}} = E\left\{\boldsymbol{\Psi}\boldsymbol{\Psi}^{\mathrm{H}}\right\} = \mathbf{G}E\left\{\boldsymbol{p}\boldsymbol{p}^{\mathrm{H}}\right\}\mathbf{G}^{\mathrm{H}} + {\sigma_e}^2\mathbf{I}. \tag{6}$$

where $\mathbf{R}_{\boldsymbol{\Psi}}$ is a Hermitian matrix of size $M \times M$. Using eigen decomposition, we obtain the following:

$$\mathbf{R}_{\boldsymbol{\Psi}} = \mathbf{U}\Sigma\mathbf{U}^{\mathrm{H}}. \tag{7}$$

where Σ is a diagonal matrix with eigenvalues $\lambda_1 \geq \lambda_2 \geq \cdots \geq \lambda_K \geq 0$. We assume that only one electric dipole source is in this locating area. As a result, the signal subspace $\mathbf{U}_{\mathrm{S}}$ is the vector space spanned by the first column of $\mathbf{U}$. The remainder of the columns compose the noise subspace $\mathbf{U}_{\mathrm{N}}$. Thus, the projection matrix of the noise subspace can be expressed as $\mathbf{P}^{\perp} = \mathbf{I} - \mathbf{U}_{\mathrm{S}}\mathbf{U}_{\mathrm{S}}^{H}$. Assuming the electric dipole source is located at position $\boldsymbol{r}_{\mathrm{t}} = \boldsymbol{r}_{\mathrm{t0}}$, the gain matrix or the array manifold $\mathbf{G}$ can be derived. Three eigen values are obtained via generalized eigen-decomposition as follows:

$$\begin{bmatrix}\lambda_{\mathrm{t1}} & & \\ & \lambda_{\mathrm{t2}} & \\ & & \lambda_{\mathrm{t3}}\end{bmatrix} = \mathrm{eigen}(\mathbf{G}^{\mathrm{H}}\mathbf{P}^{\perp}\mathbf{G}, \mathbf{G}^{\mathrm{H}}\mathbf{G}) \tag{8}$$

where the three eigen values are ordered as follows: $\lambda_{\mathrm{t1}} \leq \lambda_{\mathrm{t2}} \leq \lambda_{\mathrm{t3}}$. The evaluation function is derived based on the

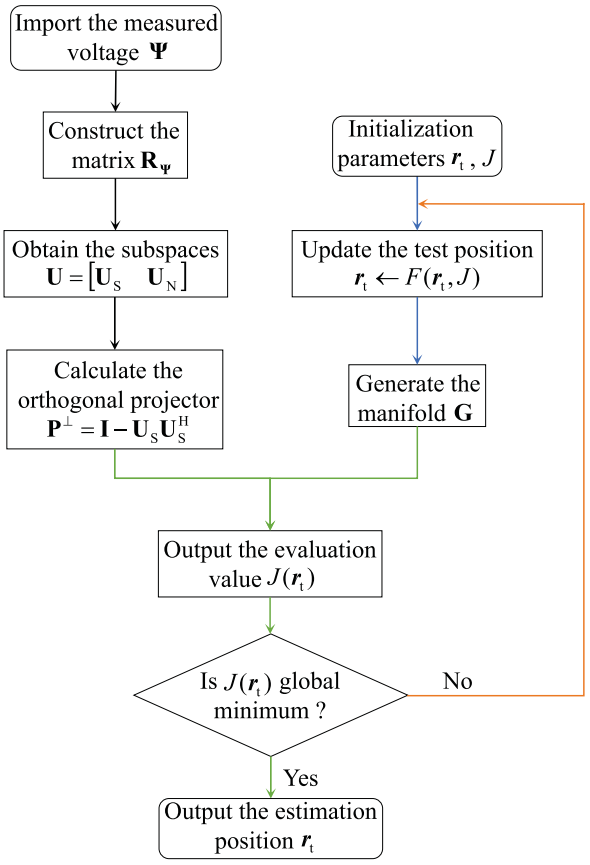

FIGURE 2. The locating flow diagram.

MP-MUSIC algorithm as follows: $J(\boldsymbol{r}_t) = \lambda_{t1}$. Alternatively, the space spectrum can be represented as $P(\boldsymbol{r}_t) = \frac{1}{J(\boldsymbol{r}_t)}$. The estimated position that minimizes the evaluation function J or maximizes the spectrum P corresponds to the position of the electric dipole source. According to the literature [26], [29], and [27], the locating flow diagram is shown in Figure 2, where the function F in the flow diagram is the optimization strategy, which could help the locating system find the position of the electric dipole source with fewer computations.

C. LOCATING THE TARGET WITH THE IMPROVED MA-ES METHOD

Locating the position of the electric dipole source is essentially an optimization problem. We can therefore choose one optimization method among the optimization algorithms. However, not all optimization algorithms are suitable to locate an underwater target. Because underwater target locating is a nonconvex optimization problem, with some local minimums, the gradient method cannot be directly applied to solve the underwater locating problem. The improved optimization method based on the improved MA-ES engine is proposed to lower the computation burden, as shown in Figure 3. In this optimization strategy proposed by Beyer and Sendhoff [30], the ellipse optimization landscape is depicted with the evaluation function J. In practice,the population (dots) is much larger than necessary. The figure

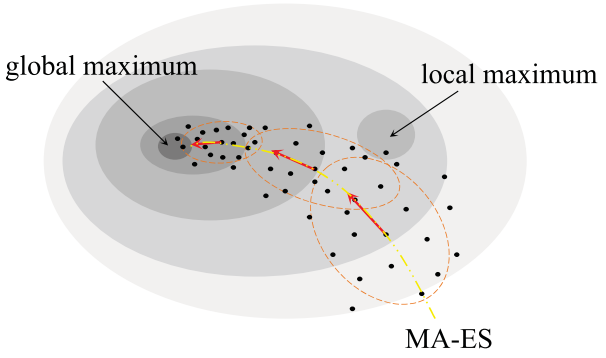

FIGURE 3. Illustration of an actual optimization run with (C)MA-ES method where the yellow dash line indicates the evaluation path by the use of MA-ES.

illustrates how the distribution of the population position (yellow dash line) moves during the optimization. In this optimization problem, the population convergences to the global optimum within a few generations.

The MA-ES algorithm includes the standard covariance matrix adaptation evolution strategy (CMA-ES), which consists of two evolution paths: 1) learning the mutation strength; and 2) the rank-one update of the covariance matrix. In his work, people can reduce two items, one of the evolution paths and the covariance matrix of the CMA-ES algorithm. As a result, the computation burden of the covariance matrix update and its square root operations is reduced [30]. To remove the covariance matrix $\mathbf{C}$ and $\mathbf{p}$-path, this algorithm is based on the assumption that $c_p = c_s$. However, in Beyer's work, the factors c_p and c_s are not equal in practice, which degrades the optimization performance. Hence, in this paper, we propose an improved MA-ES algorithm, where c_p and c_s are near one another. The default factors c_p and c_s are expressed as follows:

$$c_p = \frac{\mu_{\text{eff}}/N + 4}{2\mu_{\text{eff}}/N + 4 + N} \tag{9}$$

$$c_s = \frac{\mu_{\text{eff}} + 2}{\mu_{\text{eff}} + 5 + N} \tag{10}$$

In this study, the search dimension is $N = 3$. Implementing $c_p = c_s$, $\mu_{\text{eff}} = 5.26$. Based on the standard parameter settings [30], the following is derived:

$$\sum_{m=1}^{\mu} w_m^2 = \frac{1}{\mu_{\text{eff}}} \tag{11}$$

$$\sum_{m=1}^{\mu} w_m = 1 \tag{12}$$

where w_m refers to the weight factor of the mth best individual of the current offspring population with λ individuals and μ represents the number of the selected offspring. Generally, the number of the selected offspring is half that of λ, yielding $\mu = \lfloor \frac{\lambda}{2} \rfloor$. With a good choice of weight factors, (11) and (12) can be satisfied simultaneously. In this study, we apply the

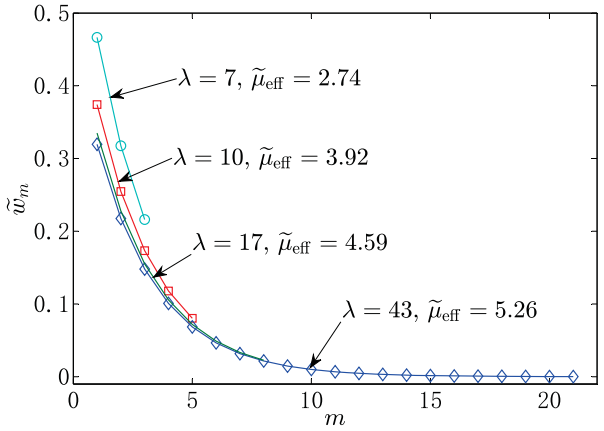

FIGURE 4. Magnetization as a function of applied field. The weight factors versus the offspring population λ.

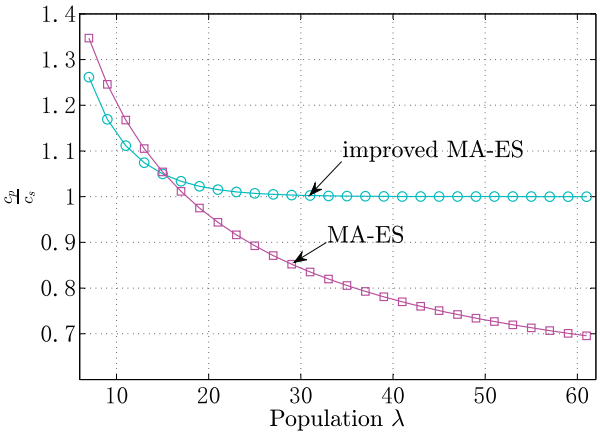

FIGURE 5. c_p/c_s ratio versus the offspring population λ.

power series weight distribution, wherein those who most fit the evaluation function are given the largest weights. Given $w_m = \alpha\eta^{m-1}$, (11) and (12) can alternatively be expressed as follows:

$$\alpha^2 \sum_{m=1}^{\mu} \eta^{2(m-1)} = \frac{1}{\mu_{\text{eff}}} \tag{13}$$

$$\alpha \sum_{m=1}^{\mu} \eta^{m-1} = 1 \tag{14}$$

According to (13) and (14), it is easy to obtain

$$\begin{cases} \alpha^2(1-\eta^{2\mu}) = \dfrac{1-\eta^2}{\mu_{\text{eff}}} \\ \alpha(1-\eta^{\mu}) = 1-\eta \end{cases} \tag{15}$$

When $\mu \to \infty$, we have $(\eta^{2\mu}, \eta^{\mu}) \to 0$. Thus, (15) can be simplified as

$$\begin{cases} \alpha^2 \approx \dfrac{1-\eta^2}{\mu_{\text{eff}}} \\ \alpha \approx 1-\eta \end{cases} \tag{16}$$

Hence, resolving (16) for α and η, $\alpha = \frac{2}{\mu_{\text{eff}}+1}$ and $\eta = \frac{\mu_{\text{eff}}-1}{\mu_{\text{eff}}+1}$. In reality, μ is not infinite, which results in $\sum_{m=1}^{\mu} w_m < 1$. Finally, the modified weight factor is as follows: $\widetilde{w}_m = \frac{\eta^{m-1}}{\sum_{i=1}^{\mu}\eta^{i-1}}$, and $\widetilde{\mu}_{\text{eff}} = \frac{1}{\sum_{i=1}^{\mu}\widetilde{w}_i^2}$. The data in Figure 4 show the weight factors for different offspring λ. These results show that the modified weight factors approaches the asymptote when $\lambda \to \infty$. As a result, $\widetilde{\mu}_{\text{eff}}$ approaches 5.26, when $\lambda \geq 43$.

In Figure 5, the ratio of c_p/c_s when using the weight factors derived with the improved MA-ES is shown. The data in this figure show that the c_p/c_s ratio depends on the distribution weight scheme. The c_p/c_s ratio cannot be near 1 when using the standard MA-ES weight scheme provided in provided in [30] and [31]. However, the weight scheme proposed in this paper shows that the c_p/c_s ratio approaches 1 as the offspring population λ increases. Moreover, the ratio does not deviate too much from 1 when $\lambda \geq 20$. The proposed weight scheme ensures that the MA-ES is suitable for different offspring populations.

The pseudocode of the improved MA-ES method, shown in Algorithm 1, is based on previous work [30]. The default strategy parameter settings are the following: 1) The learning rate of rank-one $c_1 = \frac{2}{N+1.3^2+\mu_{\text{eff}}}$; 2) Rank-$\mu$ $c_w = \min\left(1-c_1, 2\frac{\mu_{\text{eff}}-2+\frac{1}{\mu_{\text{eff}}}}{(N+2)^2+\mu_{\text{eff}}}\right)$; and 3) The damping constant $d_\sigma = 1 + c_s + 2\max\left(0, \sqrt{\frac{\mu_{\text{eff}}-1}{N+1}} - 1\right)$. In the algorithm, $\mathcal{N}(\mathbf{0}, \mathbf{I})$ represents the N-dimensional isotropically independent identically normal distribution, and the operation $\langle\cdot\rangle_{\boldsymbol{w}_\mu}$ means the following: $\langle \boldsymbol{x} \rangle_{\boldsymbol{w}_\mu} = \sum_{i=1}^{\mu} w_i \boldsymbol{x}_{m;\lambda}$.

In this section, the underwater electric dipole source locating problem is transformed to an optimization problem. As a result, three models are provided: 1) the forward model f based on the image principle, which features a small computation burden and is easily implemented; 2) the evaluation foundation J based on the MP-MUSIC algorithm, which can reduce the search dimension from 6 degrees of freedom (3 dimensions of the target position and 3 dimensions of the target azimuth) to 3 degrees of freedom (3 dimensions of target position); and 3) the improved optimization strategy F based on the low-complexity MA-ES.

III. NUMERICAL EXAMPLES

A. SIMULATION MODEL SETUP

In this section, we present a simulation model to analyze the performance of the proposed localization method. In this simulation model, the ambient conductivity is $\sigma = 4$S/m, which is the same as that of the seawater. In a practical application, we cannot implement a PUCA with an infinite plane. Therefore, a rectangular flat panel is built as the base of the PUCA, with length α, width β and thickness h. Seven

Algorithm 1 Improved MA-ES

Require: $\boldsymbol{\Psi}$, $\boldsymbol{r}_{\mathrm{t}0}$, $\sigma^{(0)}$, σ_{stop}, λ; % input the raw data and information of the environment

Ensure: $\boldsymbol{r}_{\mathrm{estimate}}$; % output the target estimation position

Initialize: $\boldsymbol{r}_{\mathrm{t}}{}^{(0)} \leftarrow \boldsymbol{r}_{\mathrm{t}0}$, $g \leftarrow 0$, $\mathbf{s}^0 \leftarrow \mathbf{0}$, $\mathbf{M}^{(0)} \leftarrow \mathbf{I}$, $\mu_{\mathrm{eff}} \leftarrow 5.26$

$\eta = \frac{\mu_{\mathrm{eff}}-1}{\mu_{\mathrm{eff}}+1}$

$w_m \leftarrow \frac{\eta^{m-1}}{\sum_{i=1}^{\mu}\eta^{i-1}}, m = 1, 2, \cdots, \mu;$

$\mu_{\mathrm{eff}} \leftarrow \frac{1}{\sum_{i=1}^{\mu} w_i^2}$

repeat

  for $l = 0$ **to** λ **do**

    $\boldsymbol{z}_l^{(g)} \leftarrow \mathcal{N}_l(0, \mathbf{I})$;

    $\boldsymbol{d}_l^{(g)} \leftarrow \mathbf{M}^{(g)}\boldsymbol{z}_l^{(g)}$;

    $J_l^{(g)} \leftarrow J(\boldsymbol{r}_{\mathrm{t}}{}^{(g)} + \sigma^{(g)}\boldsymbol{d}_l^{(g)})$

  end for

  Sort the offspring population in decrease order

  $\boldsymbol{r}_{\mathrm{t}}{}^{(g+1)} \leftarrow \boldsymbol{r}_{\mathrm{t}}{}^{(g)} + \sigma^{(g)}\left\langle \boldsymbol{d}^{(g)}\right\rangle_{\boldsymbol{w}_\mu}$

  $\boldsymbol{s}^{(g+1)} \leftarrow (1-c_s)\boldsymbol{s}^{(g)} + \sqrt{\mu_{\mathrm{eff}}c_s(2-c_s)}\left\langle \boldsymbol{z}^{(g)}\right\rangle_{\boldsymbol{w}_\mu}$

  $\mathbf{C}_1 = \frac{c_1}{2}\left(\boldsymbol{s}^{(g+1)}(\boldsymbol{s}^{(g+1)})^{\mathrm{T}} - \mathbf{I}\right)$

  $\mathbf{C}_w = \frac{c_w}{2}\left(\left\langle \boldsymbol{z}_l^{(g)}(\boldsymbol{z}_l^{(g)})^{\mathrm{T}}\right\rangle_{\boldsymbol{w}_\mu} - \mathbf{I}\right)$

  $\mathbf{M}^{(g+1)} \leftarrow \mathbf{M}^{(g)}\left[\mathbf{I} + \mathbf{C}_1 + \mathbf{C}_w\right]$

  $\sigma^{(g+1)} \leftarrow \sigma^{(g)}\exp\left[\frac{c_s}{d_\sigma}\left(\frac{\|\boldsymbol{s}^{(g+1)}\|}{\mathrm{E}[\|\mathcal{N}(\mathbf{0},\mathbf{I})\|]} - 1\right)\right]$

  $g++$

until Fulfill termination conditions

$\boldsymbol{r}_{\mathrm{estimate}} = \boldsymbol{r}_{\mathrm{t}}$

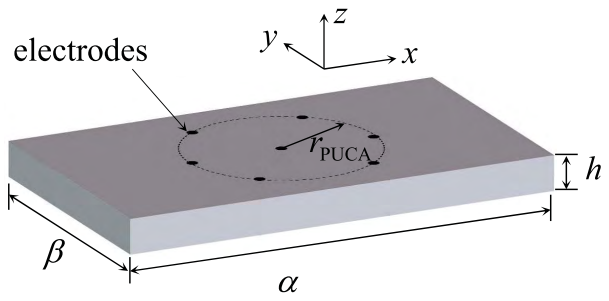

FIGURE 6. The improved PUCA system with 7 receiving electrodes.

electrodes are located on the rectangular flat panel, forming a receiving antenna array. Electrodes with index number 1 to 6 are uniformly distributed in a circle of radius $r_{\mathrm{PUCA}} = 8$ cm. The seventh electrode is the reference electrode, which is set at the center of the panel. The voltage between the m th electrode and the reference electrode is the received data of channel m, where $m = 1, 2, 3, 4, 5, 6$. The structure of the PUCA is shown in Figure 6. Table 1 shows the position of each electrode. Theoretically, the forward model for this rectangular flat panel would not be the same as the forward model f in (2) because the boundary condition changes.

TABLE 1. The positions of the 7 electrodes in the PUCA system.

Index	1	2	3	4	5	6	7
x (cm)	8.00	4.00	-4.00	-8.00	-4.00	4.00	0
y (cm)	0	-6.93	-6.93	0	6.93	6.93	0
z (cm)	0	0	0	0	0	0	0

However, the image principle-based forward model f yields an approximate solution that is sufficiently accurate for practical applications when the panel boundary effect can be neglected.

We first investigate the accuracy of the proposed forward model f as the size parameters of the panel change. An electric dipole source is located at position (0, 0, 10) (cm). The low-frequency time harmonic signal of 1kHz is loaded on the dipole. The dipole moment is $\boldsymbol{p} = (0, 0, 1)$. We calculate the voltage from channel 1 and channel 2 of the PUCA versus the structure parameters α and β when $h = 1$ cm using the commercial electromagnetic simulator environment computer simulation technology (CST) Studio Suite and the proposed forward model f (the electric dipole source and the PUCA compose a symmetrical system; therefore, the voltages of channels 1 and 4 are the same, and channels 3, 5 and 6 have the same voltages as channel 2). The voltages are shown in Figure 7, and a selection of the simulation results are listed in Tables 2 and 3. The data in Figure 7 and Tables 2 and 3 show that the voltages obtained by the forward model f are similar to the results via CST, i.e., the error is less than 1% when $\min(\alpha, \beta) \geq 3\, r_{\mathrm{PUCA}}$. However, the data show a relatively large error when $\min(\alpha, \beta) \leq 2.5\, r_{\mathrm{PUCA}}$, i.e., the error is greater than 3%. We varied the electric dipole source position (0, 0, z) from $z = 8$ (cm) to $z = 30$ (cm). From Figure 8, the voltages obtained by the forward model f show good match with the results from CST when the electric dipole source is situated at different positions.

TABLE 2. The voltage ratio from the CST and the voltages from the forward model f for channel 1.

β (cm)	20	26	30	60
$\alpha = 20$ cm	1.039	1.052	1.052	1.057
$\alpha = 30$ cm	0.996	1.002	1.005	1.008
$\alpha = 40$ cm	0.990	0.996	0.999	1.004
$\alpha = 60$ cm	0.988	0.996	0.998	1.000

TABLE 3. The voltage ratio from the CST and the voltages from the forward model f for channel 2.

β (cm)	20	26	30	60
$\alpha = 20$ cm	1.022	1.006	1.000	1.000
$\alpha = 30$ cm	1.030	1.008	1.004	0.999
$\alpha = 40$ cm	1.030	1.009	1.005	1.002
$\alpha = 60$ cm	1.029	1.010	1.006	1.000

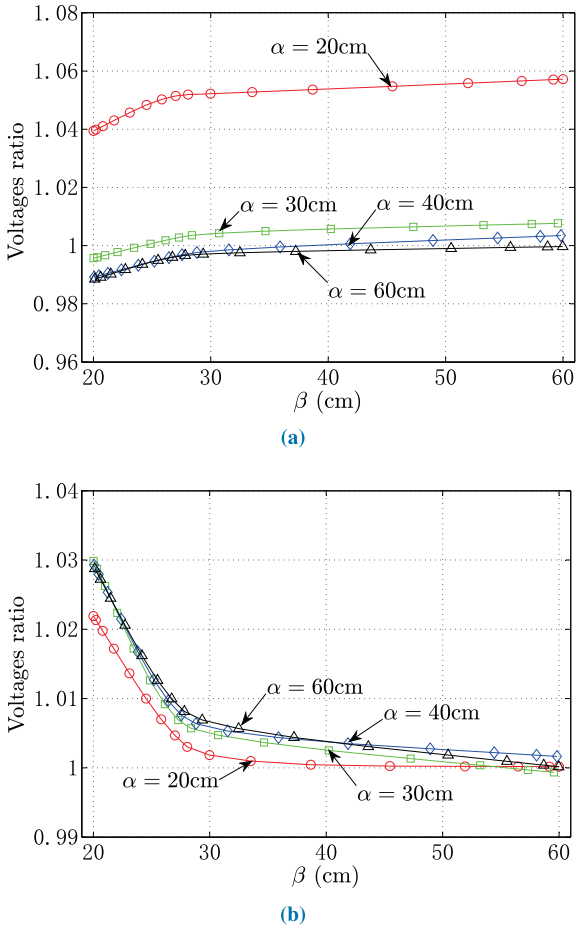

FIGURE 7. The ratio of the voltages from the CST and the voltages from the forward model f. (a) The voltage ratio of channel 1; (b) The voltage ratio of channel 2.

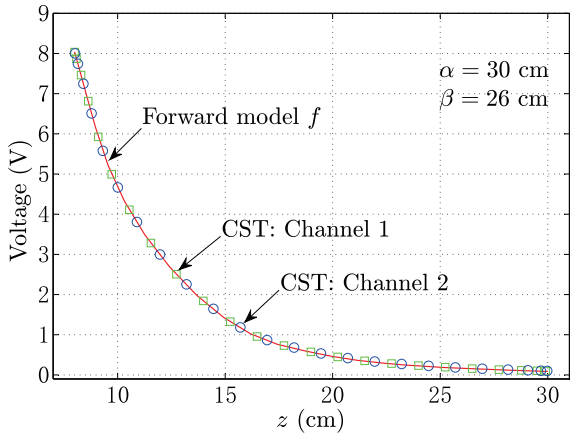

FIGURE 8. The voltages obtained by the forward model f and CST when $\alpha = 30$ cm and $\beta = 26$ cm.

A locating system is usually placed on an autonomous underwater vehicle (AUV), which means that the structure parameter h is determined by the carrier. Hence, the influence of structure parameter h should also be taken into consideration. The data in Figure 9 show the voltages ratio from channels 1 and 2 with different h when the electric dipole source is placed at point (0, 0, 10) (cm) with $\alpha = 30$ cm and $\beta = 26$ cm. The results show that the two curves approach 1, and the panel thickness h has no significant influence on the calculation results from channels 1 and 2, with the maximum error less than 0.3%, which means that the influence of the factor h can be neglected.

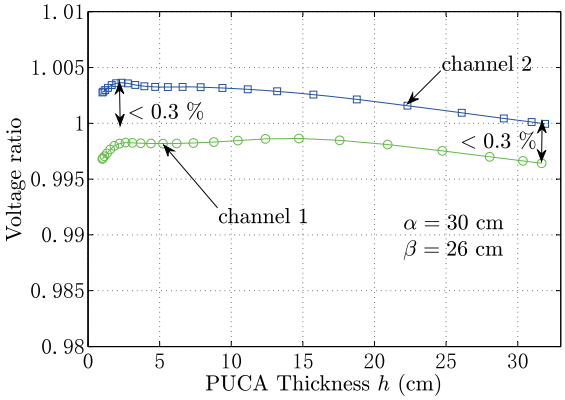

FIGURE 9. The voltage ratio by the forward model f and CST versus the panel thickness h, when $\alpha = 30$ cm and $\beta = 26$ cm.

From this subsection, we conclude that the proposed forward model f based on the image principle is simple in expression, resulting in a small computation burden. According to the CST analysis, the forward model results in the accurate voltage for each channel of the designed PUCA for underwater electric dipole source locating, thus verifying the proposed forward model.

B. UNDERWATER LOCATING PERFORMANCE

The space spectrum P is plotted versus the measured voltage from the PUCA system. By finding the peak of P, the target can be located. To simulate the practical scenario, the received data from the PUCA are mixed with additive white Gaussian noise. In this simulation, the squared "F" norm of the signal matrix $\|\mathbf{Gp}\|_{\mathrm{F}}^2$ is one hundred times that of the squared "F" norm of the noise matrix $\|\boldsymbol{e}\|_{\mathrm{F}}^2$, yielding a signal-to-noise ratio (SNR) of 20 dB [32], [33]. We set the electric dipole source at positions (0, 10, 10) cm, (30, 10, 10) cm and (30, 20, 20) cm. Spectrum images are thus obtained and shown in Figure 10. In the images, the green points are the actual location of the source. The highlighted points represent the estimated positions of the source, which are (0, 9.67, 10.02) cm, (31.71, 10.37, 6.16) cm, and (31.54, 20.58, 18.68) cm. The spectrum is not a convex function, i.e., there is more than one local maximum in the spectrum, as shown in Figure 10 (a). Hence, the solution can easily be trapped in a local maximum using a gradient-based algorithm.

In this subsection, we focus on the performance of the improved optimization strategy when the evaluation function J is minimized. Providing that the electric dipole source

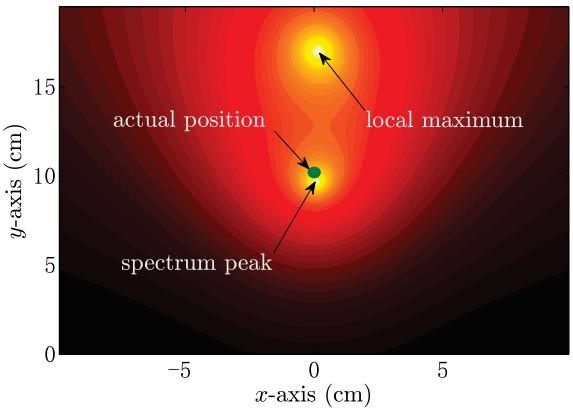

(a)

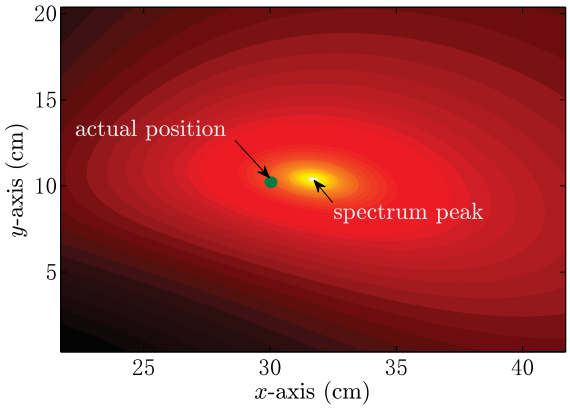

(b)

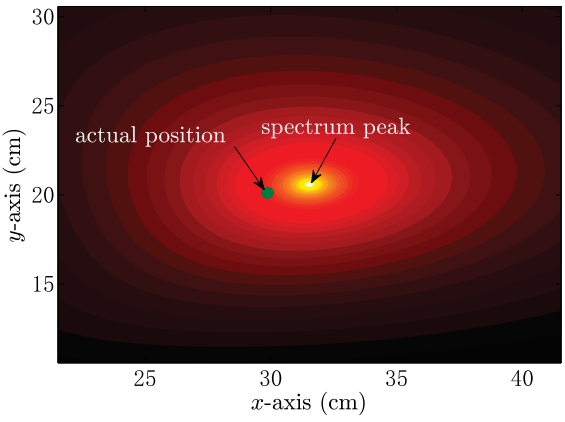

(c)

FIGURE 10. The spectrum images are given based on the MP-MUSIC results when SNR = 20 dB. (a) The real position of the electric dipole source is (0, 10, 10) cm; (b) The real position of the electric dipole source is (30, 10, 10) cm; (c) The real position of the electric dipole source is (30, 20, 20) cm.

is located at point (0, 10, 10) cm with a dipole moment of (1, 1, 0) A·m. All the simulations run on a laptop with the following configuration: Intel Core i3−4030U CPU @1.9 GHz, 4 GB RAM, Windows 10 (64 bit) operating system and MATLAB 2010b. We first analyze the performance of the

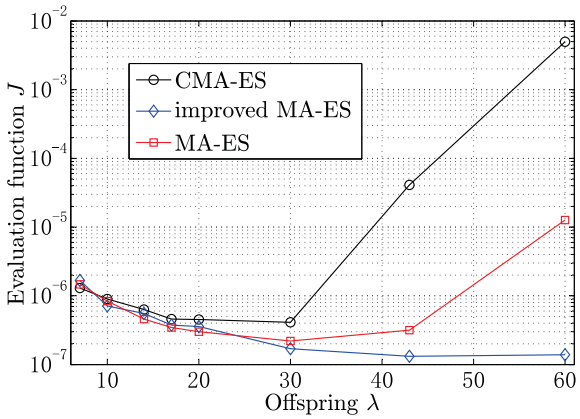

FIGURE 11. The evaluation function J with different offspring population λ.

optimization strategies (CMA-ES, MA-ES and the improved MA-ES) when the total number of calculations is 18000, yielding $\frac{18000}{\lambda}$ generations. The average J, after 100 simulations, is shown in Figure 11. The data show that the three optimization strategies show similar performance when $\lambda \leq 30$. However, the optimization performances of CMA-ES and MA-ES degrade when $\lambda \geq 30$. That is because the offspring generation decreases when λ increases, resulting in inadequate adaptation. The data for the improved MA-ES show better optimization performance, indicating that the optimization result is not significantly affected by λ.

The convergence speed is also considered. In Figure 12(a), the offspring population is set at $\lambda = 43$, and the average evaluation value decreases as the number of evolution generations increases. The improved MA-ES convergences more rapidly to 10^{-7} when the evolution generations is larger than 360. The optimization results will not decrease significantly when the number of evolution generations is larger than 400. However, more than 500 and 550 generations are required for the convergence of the MA-ES and the CMA-ES, respectively, with stable optimization results larger than 10^{-6}. One can see that the average locating errors estimated by the optimization strategies show strong correlation with the evolution generation of the offspring from Figure 12 (b). The average estimating error using the improved MA-ES can be as large as 0.02 cm, when the number of generations is larger than 360. The MA-ES results have an estimating error greater than 0.025 cm, where the number of generations is greater than 430. Using CMA-ES, the number of evolution generations must be greater than 600 to achieve an estimation error of approximately 0.025 cm. Both the MA-ES and the improved MA-ES require similar calculation times for the same number of evolution generations, yielding 8.3 ms per generation, as shown in Figure 12 (c). For similar accuracy in the results, the CMA-ES requires 9 ms per generation. Compared with the two optimization strategies (CMA-ES and MA-ES), with respect to convergence speed and computation

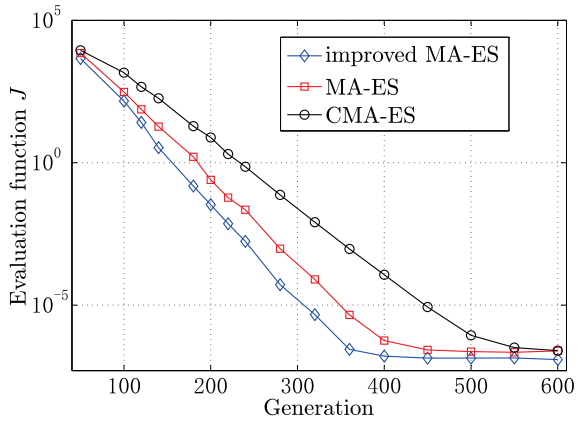

(a)

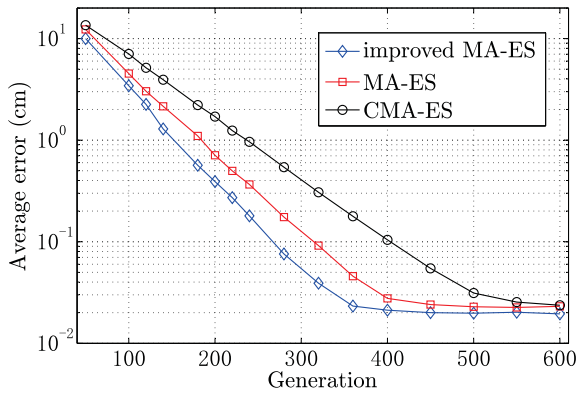

(b)

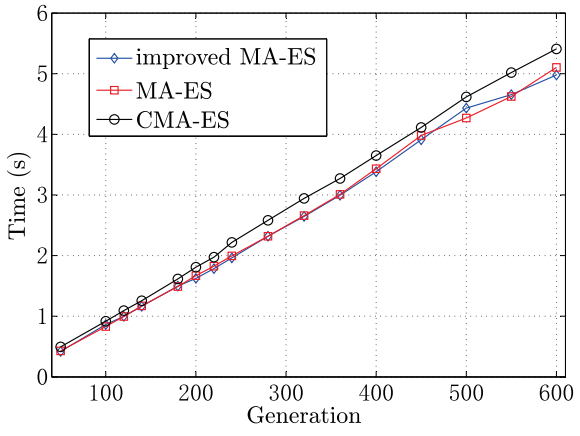

(c)

FIGURE 12. The performance of the optimization strategies when $\lambda = 43$. (a) The evaluation function J versus offspring generation; (b) The estimated position errors; (c) The calculation time versus offspring generation.

burden, the improved MA-ES yields a better solution and has a smaller computation burden.

Further study of the proposed PUCA system shows that the image principle can accurately describe the electric field distribution of the panel-based PUCA system. Moreover, the thickness of the panel has little effect on the electric field distribution. The evolution function J, based on MP-MUSIC, shows that the global minimum corresponds to the position of the electric dipole source. However, the proposed underwater locating method is a non-convex optimization, resulting in local minimums in the evolution function, indicating that a global optimization strategy must be applied. The improved MA-ES is introduced and analyzed in detail, resulting in a faster convergence speed than the MA-ES or the CMA-ES. Moreover, the improved MA-ES has a similar computation burden as MA-ES and a lower computation burden than the classical CMA-ES because the operations to generate the covariance matrix and to calculate the matrix square root are reduced, which simplifies the evolution strategy significantly both from the algorithmic complexity and the computation burden. The improved MA-ES also provides a more accurate solution than both the MA-ES and the CMA-ES.

IV. EXPERIMENT

The physical experiment is performed in our laboratory environment to verify the proposed locating method. The PUCA system is designed with seven electrodes. An image of the PUCA system is shown in Figure 13. The receiving electrodes' positions are listed in Table 1, and the diameter is

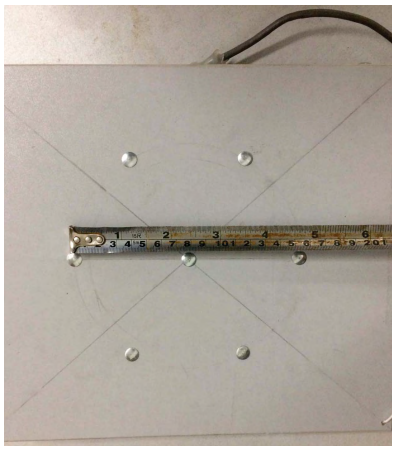

(a)

(b)

FIGURE 13. (a)The image of the PUCA system; (b) The electric dipole source.

11 mm. The panel of the PUCA system is plastic with the following structural parameters: $\alpha = 30$ cm, $\beta = 26$ cm and $h = 1$ cm. In this experiment, the PUCA is horizontally floating in the center of the water tank shown in Figure 14. The water tank fills with water creating a body of water with length of 3 m, width of 1.5 m and height of 1.5 m. Sea salt is added to the water, and we adjust the conductivity to 4 S/m, which is similar to the conductivity of seawater. Two metal sheets that cover the end of a cylindrical plastic pipe (length 12 cm, radius 10 mm) act as the electric dipole source, which is fixed to a horizontal movable gantry workbench on the tank. We can move the dipole source to any point in the tank with high resolution. In this experiment, the measured impedance of the electric dipole source in water is 20 Ω at 1 kHz. The load voltage of the dipole source is 1.04 Vrms, yielding a dipole moment of 6 mA · m. Restricted by the experimental equipment, the time division measurement method and the offline locating method are

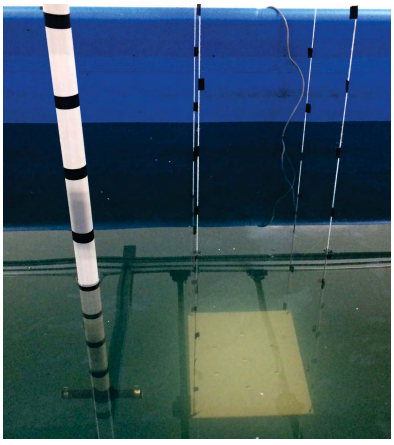

(a)

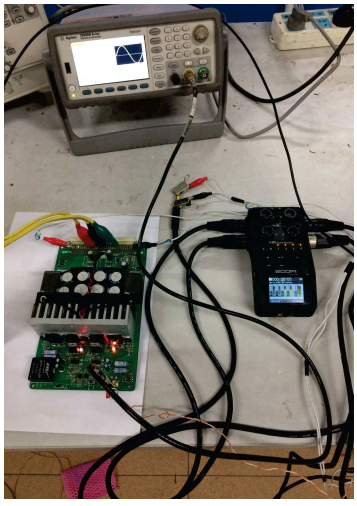

(b)

FIGURE 14. (a) The physical experiment environment; (b) The amplifier of the electro-locator and the ZOOM H6 Handy Recorder with configurable gain from $-\infty$ to 55.5 dB with a 96 kHz sample rate and 24 bit precision.

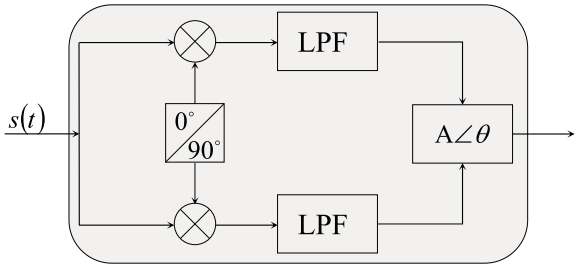

FIGURE 15. The schematic diagram of the digital narrow band demodulation filter.

adopted. The seven electrodes compose six channel receivers, from channel 1 to channel 6. The high-precision voltage measurement meter ZOOM H6 Handy Recorder is used to sample and store the measured voltage data, which then is imported into the MATLAB calculator. During the voltage measuring, channel *i* is connected to the input 1 of the ZOOM H6 Handy Recorder. Meanwhile, channel 4 is connected to the input 2 of ZOOM H6 Handy Recorder as the signal phase reference. In this manner, the voltages of channels *i* and 2 are measured and stored simultaneously.

We set the electric dipole source above the PUCA at the plane $z = 20$ cm. According to the measurements, the voltage from the PUCA is in the range of $0.1 \sim 8.0$ mV, and the data contain noise. Thus, if we only use the measured data from one snapshot, the SNR would be low because of the wide sampling band, which might result in locating failure. To reduce the out-of-band noise and interference, a digital narrow-band demodulation filter is applied to the background to extract the voltage magnitude. To reduce the additional gain and phase distortion, each channel of the PUCA uses a controllable digital filter with the same parameters. The MATLAB FDATOOL is used to generate the filter coefficients. The generation of filter coefficients is achieved using a frequency mixing operation to shift the signal to the baseband. The baseband signal then passes through a narrow-band low-pass filter, resulting in a very high rejection of out-of-band signals [34]. The filter outputs the voltage and the angle of each channel with high SNR, which can be used as input data to the evaluation function J with only one snapshot. A schematic diagram of the digital narrow-band demodulation filter is shown in Figure 15. In this system, the bandpass of the filter is 400 Hz. The filtered data are shown in Figure 16, where the noise is significantly reduced by the digital filter.

An example will illustrate the proposed locating method step by step. The measured raw data are the input arguments to the electro-locator, and the electro-locator will export the electric dipole position after the calculation as follows:

- **Step 1:** Load the measured data $\mathbf{\Psi}_{\mathrm{m}}$ from https://drive.google.com/file/d/1fAOm2r9CKQ2SgjRmZ3J3qfzfKcOIWfQo/view?usp=sharing;
- **Step 2:** Filter the measured voltage with the demodulation narrow-band filter. Output the amplitude and

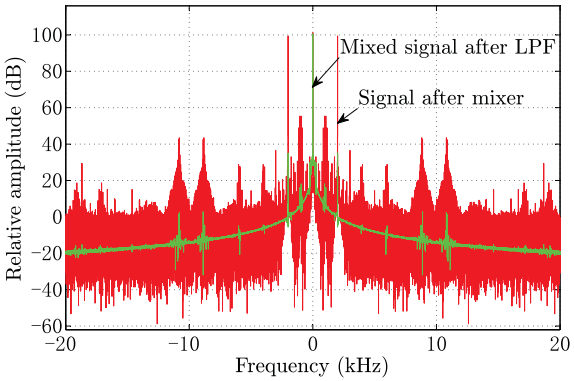

FIGURE 16. Red: The frequency spectrum of the measured voltage after the mixer; Green: The measured data after the low pass filter (LPF).

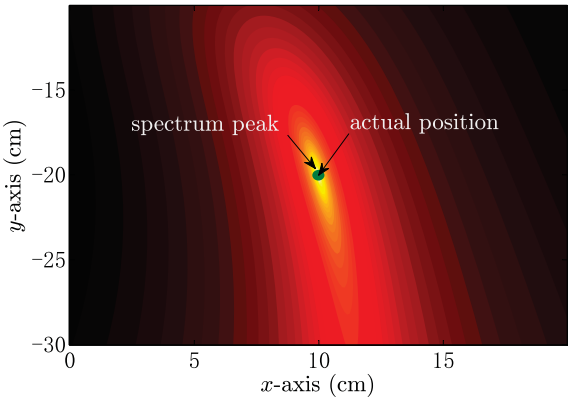

FIGURE 17. The space spectrum at the plane $z = 22.2$ cm.

angle of channel i and phase reference channel 4. The resulting voltage ratios, $\frac{\psi_i}{\psi_4}$: $\frac{\psi_1}{\psi_4} = -0.447$, $\frac{\psi_2}{\psi_4} = 0.0629$, $\frac{\psi_3}{\psi_4} = 0.989$, $\frac{\psi_4}{\psi_4} = 1.00$, $\frac{\psi_5}{\psi_4} = 0.731$, and $\frac{\psi_6}{\psi_4} = 0.180$, yield the modified data $\mathbf{\Psi} = [-0.447\ 0.0629\ 0.989\ 1.00\ 0.731\ 0.180]^{\mathrm{T}}$;

- **Step 3:** Calculate the covariance matrix

$$R_{\mathbf{\Psi}} = \kappa \begin{pmatrix} 2.0 & -0.28 & -4.4 & -4.5 & -3.3 & -0.80 \\ -0.28 & 0.04 & 0.62 & 0.63 & 0.46 & 0.11 \\ -4.4 & 0.62 & 9.8 & 9.9 & 7.2 & 1.8 \\ -4.5 & 0.63 & 9.9 & 10.0 & 7.3 & 1.8 \\ -3.3 & 0.46 & 7.2 & 7.3 & 5.3 & 1.3 \\ -0.80 & 0.11 & 1.8 & 1.8 & 1.3 & 0.32 \end{pmatrix},$$

where κ is a real number that is larger than zero;

- **Step 4:** Obtain the eigenvector $\mathbf{U}$, and the eigenvalue $\mathbf{\Sigma}$ using eigenvalue decomposition. In this example,

$$\mathbf{U} = 0.1 \begin{pmatrix} -0.35 & -1.4 & 9.5 & 0.62 & 0.98 & -2.7 \\ 0.15 & 0.38 & 0.78 & -9.9 & 0.46 & 0.38 \\ -1.5 & -2.6 & 2.0 & -0.072 & -7.2 & 6.0 \\ 2.1 & 6.7 & 2.4 & 0.84 & 2.8 & 6.0 \\ -3.2 & -5.5 & -0.34 & 0.17 & 6.3 & 4.4 \\ 9.1 & -4.0 & 0.004 & 0.042 & 0.43 & 1.1 \end{pmatrix},$$

$$\mathbf{\Sigma} = \beta \begin{pmatrix} 0 & 0 & 0 & 0 & 0 & 0 \\ 0 & 0 & 0 & 0 & 0 & 0 \\ 0 & 0 & 0 & 0 & 0 & 0 \\ 0 & 0 & 0 & 0 & 0 & 0 \\ 0 & 0 & 0 & 0 & 0 & 0 \\ 0 & 0 & 0 & 0 & 0 & 2.75 \end{pmatrix},$$

where β is a real number greater than zero. Therefore, the signal subspace is

$$\mathbf{U}_{\mathrm{S}} = \begin{pmatrix} -0.27 \\ 0.038 \\ 0.60 \\ 0.60 \\ 0.44 \\ 0.11 \end{pmatrix},$$

and the noise subspace projection matrix is

$$\mathbf{P}^{\perp} = 0.1 \begin{pmatrix} 9.3 & 0.10 & 1.6 & 1.6 & 1.2 & 0.29 \\ 0.10 & 10.0 & -0.23 & -0.23 & -0.17 & -0.04 \\ 1.6 & -0.23 & 6.4 & -3.6 & -2.6 & -0.65 \\ 1.6 & -0.23 & -3.6 & 6.4 & -2.7 & -0.65 \\ 1.2 & -0.17 & -2.6 & -2.7 & 8.1 & -0.48 \\ 0.29 & -0.04 & -0.65 & -0.65 & -0.48 & 9.9 \end{pmatrix};$$

- **Step 5:** Set the initial point at $(0, 0, 5)$, and start the improved MA-ES engine. For a more straightforward expression, we use the spectrum P near the electric dipole source, as shown in Figure 17;
- **Step 6:** The final output of the improved MA-ES optimization result is $(10.0, -20.0, 24.1)$, which is near the true position $(10, -20, 20)$.

In Table 4, the estimated positions and their actual positions are listed, where all the estimated positions are near the corresponding actual positions. However, the last row shows a maximum error of 8.1 cm. The estimation errors are caused by the following four reasons: 1) the electric dipole source in the experiment is not an ideal dipole; therefore, using the ideal dipole model may generate an error; 2) the proposed locating method is suitable for deep sea target locating; however, the experiment is implemented in a water tank, wherein the boundary can affect the distribution of the electric field, resulting in errors; 3) the actual positions of the electric dipole source and the PUCA system may move slightly during the measurements from the action of the water

TABLE 4. The estimated positions of the conductor target and insulator target in different positions.

Index	Actual Position	Estimated Position	Error (cm)
1	$(0, -20, 20)$	$(-1.1, -17.0, 16.1)$	5.0
2	$(10, -20, 20)$	$(10.0, -20.0, 24.1)$	4.1
3	$(10, -30, 20)$	$(10.2, -29.0, 17.1)$	3.1
4	$(20, -30, 20)$	$(20.1, -35.3, 21.2)$	5.4
5	$(20, -50, 20)$	$(11.9, -50.1, 20.4)$	8.1

wave; and 4) the SNR decreases as the distance between the electric dipole source and the PUCA decreases, degrading the locating performance. Although some experimental results slightly offset the center position, the localization accuracy is still good. These results prove that the proposed localization scheme can be applied for underwater target locating.

V. CONCLUSIONS

In this paper, we propose a novel target locating method based on the optimization method in an underwater environment. As one of the three elements of the optimization method, the forward model f, based on the image principle, is proposed. The PUCA for the locating sensors is designed and studied using CST. The results show that the electric field distribution on the panel of the PUCA with a finite volume can be described with the image principle-based forward model f when $\min(\alpha, \beta) \geq 3$. Furthermore, the effect of the thickness h of the panel can be neglected. The forward model f is a simple expression, yields high accuracy for the PUCA, and has a small computation burden. MP-MUSIC is introduced as the evaluation function J for another element of the optimization method, which can reduce the search space dimension (from six dimensions to three dimensions). The electric dipole source is located by determining the optimal solution of the evaluation function J or by finding the peak of the space spectrum P. Hence, the improved MA-ES for the optimization method is proposed. The improved MA-ES provides better performance in convergence, uses 28% fewer evaluation generations as compared with the MA-ES, and outputs a more accurate solution. Moreover, the MA-ES based algorithm has a smaller computation burden, i.e., the calculation amount is less than that of the CMA-ES by 7.8%. A set of physical experiments is performed in a water tank to verify the proposed locating method. In this experiment, a PUCA system is implemented, which consists of a plastic panel base and seven electrodes (corresponding to six receiving channels), acting as the sensor. The sampling signal is filtered using a digital demodulation narrow-band filter, which provides a high SNR base band signal for each channel. The experiments provide satisfactory locating results, verifying the effectiveness of the proposed locating method.

REFERENCES

[1] F. Boyer, V. Lebastard, C. Chevallereau, and N. Servagent, "Underwater reflex navigation in confined environment based on electric sense," *IEEE Trans. Robot.*, vol. 29, no. 4, pp. 945–956, Aug. 2013.

[2] S. Bazeille, V. Lebastard, S. Lanneau, and F. Boyer, "Model based object localization and shape estimation using electric sense on underwater robots," *IFAC-PapersOnLine*, vol. 50, no. 1, pp. 5047–5054, 2017.

[3] V. Lebastard, F. Boyer, and S. Lanneau, "Reactive underwater object inspection based on artificial electric sense," *Bioinspiration Biomimetics*, vol. 11, no. 4, p. 045003, 2016.

[4] R. Lefort, G. Real, and A. Drémeau, "Direct regressions for underwater acoustic source localization in fluctuating oceans," *Appl. Acoust.*, vol. 116, pp. 303–310, Jan. 2017.

[5] B. Li, S. Zhou, M. Stojanovic, L. Freitag, and P. Willett, "Multicarrier communication over underwater acoustic channels with nonuniform Doppler shifts," *IEEE J. Ocean. Eng.*, vol. 33, no. 2, pp. 198–209, Apr. 2008.

[6] E. M. White, J. C. Partridge, and S. C. Church, "Ultraviolet dermal reflexion and mate choice in the guppy, *Poecilia reticulata*," *Animal Behav.*, vol. 65, no. 4, pp. 693–700, Apr. 2003.

[7] S. Bardhan and S. Jacob, "Experimental observation of direction-of-arrival (DOA) estimation algorithms in a tank environment for sonar application," in *Proc. Int. Symp. Ocean Electron. (SYMPOL)*, Nov. 2015, pp. 1–6.

[8] A. G. Sazontov, I. P. Smirnov, and A. L. Matveev, "Source localization in a shallow-water channel with a rough surface," *Acoust. Phys.*, vol. 61, no. 1, pp. 109–116, 2015.

[9] H. Esmaiel and D. Jiang, "Review article: Multicarrier communication for underwater acoustic channel," *Int. J. Commun. Netw. Syst. Sci.*, vol. 6, no. 8, pp. 361–376, 2013.

[10] D. Park, K. Kwak, J. Kim, and W. K. Chung, "Underwater sensor network using received signal strength of electromagnetic waves," in *Proc. IEEE/RSJ Int. Conf. Intell. Robots Syst. (IROS)*, Hamburg, Germany, Sep. 2015, pp. 1052–1057.

[11] G. Quintana-Díaz *et al.*, "Underwater electromagnetic sensor networks—Part I: Link characterization," *Sensors*, vol. 17, no. 1, p. 189, 2017.

[12] E. F. Soderberg, "ELF noise in the sea at depths from 30 to 300 meters," *J. Geophys. Res.*, vol. 74, no. 9, pp. 2376–2387, 1969.

[13] J. Zazo *et al.*, "Underwater electromagnetic sensor networks, part II: Localization and network simulations," *Sensors*, vol. 16, no. 12, p. 2176, 2016.

[14] D.-A. Duecker *et al.*, "Embedded spherical localization for micro underwater vehicles based on attenuation of electro-magnetic carrier signals," *Sensors*, vol. 17, no. 5, p. 959, 2017.

[15] V. Lebastard *et al.*, "Underwater robot navigation around a sphere using electrolocation sense and Kalman filter," in *Proc. IEEE/RSJ Int. Conf. Intell. Robots Syst.*, Taipei, Taiwan, Oct. 2010, pp. 4225–4230.

[16] K. Wang, K. D. Do, and L. Cui, "Underwater active electrosense: A scattering formulation and its application," *IEEE Trans. Robot.*, vol. 33, no. 5, pp. 1233–1241, Oct. 2017.

[17] F. Shirmehenji, A. Z. Nezhad, and Z. H. Firouzeh, "Object locating in anisotropic dielectric background using MUSIC algorithm," in *Proc. 8th Int. Symp. Telecommun. (IST)*, Sep. 2016, pp. 396–400.

[18] Y. Xu, W. Shang, L. Guo, J. Qi, Y. Li, and W. Xue, "Active electro-location of objects in the underwater environment based on the mixed polarization multiple signal classification algorithm," *Sensors*, vol. 18, no. 2, p. 554, 2018.

[19] H. Ammari, E. Iakovleva, and D. Lesselier, "A MUSIC algorithm for locating small inclusions buried in a half-space from the scattering amplitude at a fixed frequency," *SIAM J. Multiscale Model. Simul.*, vol. 3, no. 3, pp. 597–628, 2005.

[20] Y. Xu, W. Xue, Y. Li, L. Guo, and W. Shang, "Multiple signal classification algorithm based electric dipole source localization method in an underwater environment," *Symmetry*, vol. 9, no. 10, p. 231, 2017.

[21] F. Shahbazi, A. Ziehe, and G. Nolte, "Self-consistent MUSIC algorithm to localize multiple sources in acoustic imaging," in *Proc. 4th Berlin Beamforming Conf.*, Berlin, Germany, Feb. 2012. [Online]. Available: http://www.bebec.eu/Downloads/BeBeC2012/Papers/BeBeC-2012-22.pdf

[22] N. Hansen and A. Ostermeier, "Adapting arbitrary normal mutation distributions in evolution strategies: The covariance matrix adaptation," in *Proc. IEEE Int. Conf. Evol. Comput.*, May 1996, pp. 312–317.

[23] O. R. Castro, R. Santana, J. A. Lozano, and A. Pozo, "Combining CMA-ES and MOEA/DD for many-objective optimization," in *Proc. IEEE Congr. Evol. Comput. (CEC)*, Jun. 2017, pp. 1451–1458.

[24] R. O. Schmidt, "Multiple emitter location and signal parameter estimation," *IEEE Trans. Antennas Propag.*, vol. 34, no. 3, pp. 276–280, Mar. 1986.

[25] G. Bienvenu and L. Kopp, "Optimality of high resolution array processing using the eigensystem approach," *IEEE Trans. Acoust., Speech, Signal Process.*, vol. 31, no. 5, pp. 1235–1248, Oct. 1983.

[26] J. C. Mosher and R. M. Leahy, "Recursive MUSIC: A framework for EEG and MEG source localization," *IEEE Trans. Biomed. Eng.*, vol. 45, no. 11, pp. 1342–1354, Nov. 1998.

[27] A. L. Kintz and I. J. Gupta, "A modified MUSIC algorithm for direction of arrival estimation in the presence of antenna array manifold mismatch," *IEEE Trans. Antennas Propag.*, vol. 64, no. 11, pp. 4836–4847, Nov. 2016.

[28] J. C. Mosher, P. S. Lewis, and R. M. Leahy, "Multiple dipole modeling and localization from spatio-temporal MEG data," *IEEE Trans. Biomed. Circuits Syst.*, vol. 39, no. 6, pp. 541–557, Jun. 1992.

[29] J. C. Mosher, R. M. Leahy, and P. S. Lewis, "EEG and MEG: Forward solutions for inverse methods," *IEEE Trans. Biomed. Eng.*, vol. 46, no. 3, pp. 245–259, Mar. 1999.

[30] H.-G. Beyer and B. Sendhoff, "Simplify your covariance matrix adaptation evolution strategy," *IEEE Trans. Evol. Comput.*, vol. 21, no. 5, pp. 746–759, Oct. 2017.
[31] N. Hansen and A. Auger, "Principled design of continuous stochastic search: From theory to practice," in *Theory and Principled Methods for the Design of Metaheuristics*. Berlin, Germany: Springer, 2014, pp. 145–180.
[32] K. Sekihara, D. Poeppel, A. Marantz, H. Koizumi, and Y. Miyashita, "Noise covariance incorporated MEG-MUSIC algorithm: A method for multiple-dipole estimation tolerant of the influence of background brain activity," *IEEE Trans. Biomed. Eng.*, vol. 44, no. 9, pp. 839–847, Sep. 1997.
[33] J. C. Mosher and R. M. Leahy, "Source localization using recursively applied and projected (RAP) MUSIC," *IEEE Trans. Signal Process.*, vol. 47, no. 2, pp. 332–340, Feb. 1999.
[34] Y. Bai, J. B. Snyder, M. Peshkin, and M. A. MacIver, "Finding and identifying simple objects underwater with active electrosense," *Int. J. Robot. Res.*, vol. 34, no. 10, pp. 1255–1277, 2015.

YIDONG XU received the B.S. degree from the College of Information and Communication Engineering, Harbin Engineering University, Harbin, China, in 2012, where he is currently pursuing the Ph.D. degree in underwater target locating.

LILI GUO received the B.S. degree from the Automation Department, Harbin Engineering University, in 1982, the M.S. degree from the Electrical Department, Nagaoka University of Technology, and the Ph.D. degree in engineering from Harbin Engineering University in 2005. He was a Research Assistant with the Tokyo University of Technology, Japan, from 1994 to 1995. He joined the University of Electro-Communications in 2006, where he was a Senior Research Scholar. He is currently a Professor with the College of Information and Communication Engineering, Harbin Engineering University. His research interests include the high-efficiency spread spectrum communication, cognitive radio theory, communication interference avoidance techniques, and underwater communication.

WENJING SHANG received the B.S. degree from the College of Machinery and Electronics, Northwest A&F University, Yangling, China, in 2013, and the M.S. degree from the College of Information and Communication Engineering, Harbin Engineering University, Harbin, China, in 2016, where she is currently pursuing the Ph.D. degree in signal processing.

YINGSONG LI (M'14) received the B.S. degree in electrical and information engineering and the M.S. degree in electromagnetic field and microwave technology from Harbin Engineering University, in 2006 and 2011, respectively, and the Ph.D. degree from the Kochi University of Technology (KUT), Japan, and Harbin Engineering University, China, in 2014. From 2016 to 2017, he was a Visiting Scholar with the University of California at Davis, Davis. He has been a Full Professor with Harbin Engineering University since 2014. He is also a Visiting Professor with Far Eastern Federal University and KUT. His recent research interests are mainly in underwater communications, signal processing, compressed sensing, and antennas. He is a senior member of the Chinese Institute of Electronics. He is an Associate Editor of the IEEE Access and *AEÜ-International Journal of Electronics and Communications*. He also serves as a reviewer for over 20 journals.